Available online at www.sciencedirect.com
ScienceDirect
Computer Physics Communications 179 (2008) 51–60
Computer Physics Communications
www.elsevier.com/locate/cpc

Simulation approaches to soft matter: Generic statistical properties vs. chemical details

Matej Praprotnik [1], Christoph Junghans, Luigi Delle Site, Kurt Kremer *

Max-Planck-Institut für Polymerforschung, Ackermannweg 10, D-55128 Mainz, Germany

Available online 30 January 2008

Abstract

The relation between atomistic structure, architecture, molecular weight and material properties is a basic concern of modern soft material science. This by now goes far beyond standard properties of bulk materials. A typical additional focus is on surface or interface aspects or on the relation between structure and function in nanoscopic molecular assemblies. This all implies a thorough understanding on many length and correspondingly time scales ranging from (sub-)atomic to macroscopic. At this point computer simulations are playing an increasingly important, if not the central role. Traditionally simulations have been separated in two main groups, namely simplified models to deal with generic or universal aspects of polymers, i.e. critical exponents, and those employing classical force field simulations with (almost) all atomistic detail, i.e. for the diffusion of small additives in a small "sample". Still characteristic problems, which require huge systems and/or long times in combination with a chemistry specific model, cannot be tackled by these methods alone. More recently with the development of scale bridging or multiscale simulation techniques, these different approaches have been combined into an emerging rather powerful tool. It is the purpose of this contribution to give a few examples of how such an approach can be used to understand specific material properties.

PACS: 02.70.Ns; 61.20.Ja; 61.25.Em

Keywords: Soft matter; Multiscale modeling; Scale bridging; Adaptive resolution simulation; Transverse DPD thermostat

1. Introduction

Synthetic and biological macromolecules, (bio-)membranes, colloidal suspensions, etc. are classified under the general term soft matter. Soft means that the characteristic energy densities, which to a first approximation are close to the elastic constants, are several orders of magnitude smaller than for conventional "hard" matter. The relevant energy scale is the thermal energy k_BT. This goes in hand with the fact that the conformational entropy of a macromolecule is of the same order as the intermolecular energy and their interplay usually determines the properties.

Macromolecules/polymers have been extensively studied on the basis of rather simple generic models. These ideas date back to the seminal work of Flory [1,2] and others and the subsequent solid theoretical basis and link to critical phenomena by de Gennes [3], who showed that all polymers follow the same universal scaling laws and that one can understand qualitatively and semi-quantitatively their behavior on the basis of scaling theories. I.e. the mean squared extension of a polymer, $R^2(N)$, follows the scaling law $\langle R^2(N)\rangle = AN^{2\nu}$, where ν is a universal critical exponent. In so-called good solvent $\nu \simeq 0.6$ ($d = 3$), while it is $1/2$ in a polymer melt. Similar relations hold for many other properties, including dynamics [3,4]. Though these power laws are universal, scaling theory says nothing about the prefactor A, which is determined by the chemical structure of the polymer and the interaction with its surrounding and can vary significantly. In certain cases ratios of prefactors can be determined in the limit of infinitely long chains. When it comes to mixtures, molecular assemblies, functional systems, etc. one is often not fully reaching the scaling regime

* Corresponding author.
E-mail addresses: praprot@mpip-mainz.mpg.de (M. Praprotnik), junghans@mpip-mainz.mpg.de (C. Junghans), dellsite@mpip-mainz.mpg.de (L. Delle Site), kremer@mpip-mainz.mpg.de (K. Kremer).
[1] On leave from the National Institute of Chemistry, Hajdrihova 19, SI-1001 Ljubljana, Slovenia.

0010-4655/$ – see front matter
doi:10.1016/j.cpc.2008.01.018

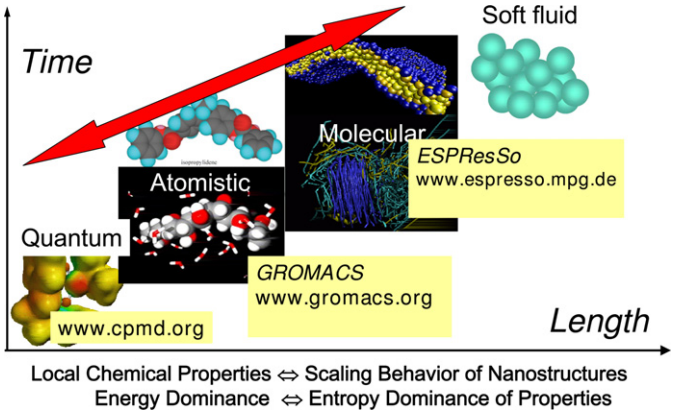

Fig. 1. Illustration of the different scales relevant for the simulation of soft matter. Open Source codes usually employed in our group for the present studies are indicated.

($N \to \infty$) and the combination of generic and chemistry specific information is absolutely conditional for any quantitative theoretical prediction. Fig. 1 illustrates the different scales and the different characteristic levels of simulation models. Many phenomena in biology, chemistry, and materials science involve processes occurring on atomistic length and time scales, which affect structural and dynamical properties on scales far beyond atomistic ones. Because it is infeasible (and most often undesirable!) to run computer simulations of very large systems with atomistically detailed models, mesoscale (coarse grained, cg) models are being developed, which stay reasonably close to the chemical structure. Reintroduction of chemical details allows to study atomistically detailed processes in various windows of the cg trajectory [5–10]. Such a procedure requires the (high- and low-) resolution models to be (pairwise) structurally consistent. However, since many high resolution states correspond one low resolution cg-state the conformational statistics on both levels of resolution should be the same if analyzed on the cg level.

In this paper we will give an overview on the scale-bridging and adaptive resolution techniques that allow for efficient computer simulations of soft matter. For a general overview of advanced computer simulation techniques we refer to Refs. [11, 12].

2. Structure-based coarse graining approach

The starting point is a mapping scheme, which simplifies the interactions significantly, while staying close enough to the chemical structure to allow for switching between scales [6,7, 10,13,14]. Fig. 2(a) (top panel) gives an example for polycarbonate (BPA-PC).

To generate the interaction potentials for the cg system we make the ansatz to strictly separate the parameterization of bonded and nonbonded interactions, based on the assumption that the total potential energy can be separated into a bonded/covalent U_B^{cg} and a nonbonded U_{NB}^{cg}. For U_B^{cg} of the cg bond and torsion angles and bond lengths we sample distribution functions of the underlying atomistic model in vacuum by a stochastic simulation, i.e. Monte Carlo. To avoid any double counting of interactions with respect to the later treated non-

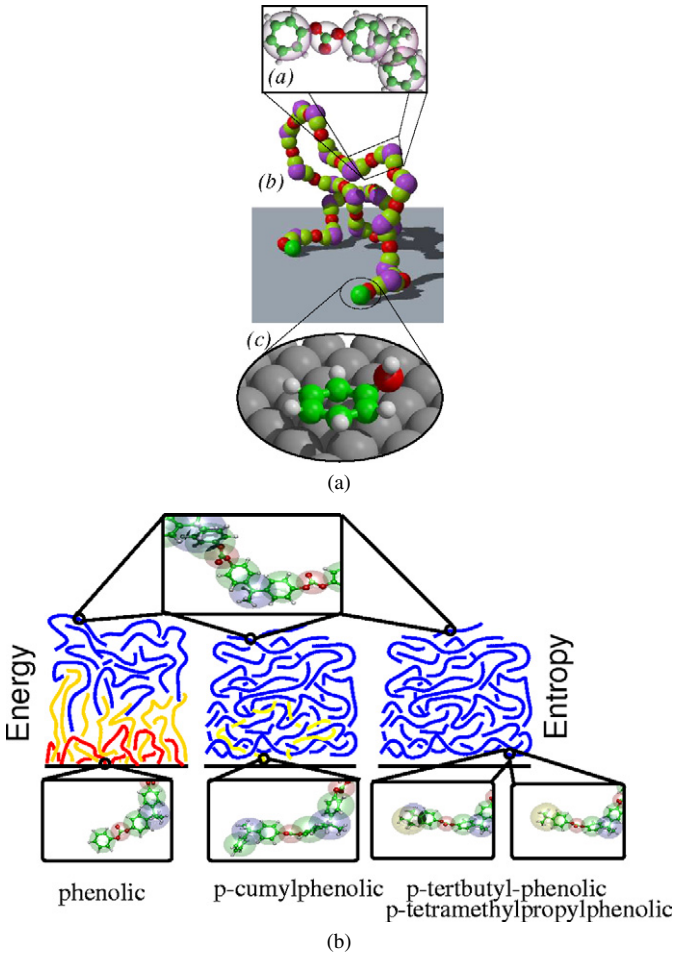

Fig. 2. (a) Illustration of the multiple scales employed to study BPA-PC at a metal surface. (b) Entropy-energy interplay for different chain terminating groups, after Ref. [15].

bonded interactions, correlations along the backbone are only considered up to the distance needed to generate the appropriate distributions. The underlying atomistic potentials preferably originate from quantum calculations, thus are not linked to any parameterization based on experiment, which typically include already further interactions. The distributions in general are characterized by the cg bond lengths r, bond angles θ, and torsions ϕ, i.e., $P(r,\theta,\phi,T)$. In many cases several different bond and torsion angles have to be considered. For simplicity, we assume $P(r,\theta,\phi,T) = P(r,T)P(\theta,T)P(\phi,T)$. This assumption generally does not hold and the choice of the cg model next to computational efficiency is tailored to minimize the introduced error, see i.e. Ref. [16]. Boltzmann inversion of the distributions yield temperature dependent bonded cg interaction potentials, i.e. for the bond length

$$U^{\mathrm{cg}}(r,T) = -k_B T \ln\left[P(r,T)/r^2\right] + const_r. \tag{1}$$

The temperature dependence concerns not only the prefactor $k_B T$ but also the distributions P themselves. Strictly speaking they can only be applied at the temperature they were derived at.

For apolar, amorphous polymers nonbonded interactions are usually sufficiently described by an excluded volume potential,

where the parameters are either estimated by group contribution methods or from the van der Waals volumes of the beads. For BPA-PC the latter was sufficient, leading to simple repulsive Lennard–Jones potentials (WCA potential) [17]. More systematically radial distributions functions of small all-atom and cg chains under appropriate melt or solution conditions are used to derive an appropriate tabulated potential by, e.g., the iterative Boltzmann inversion method [18,19]. For BPA-PC a characteristic ratio $\langle R_G^2 \rangle / N \approx 37$ Å^2, where R_G is the radius of gyration and N the number of repeat units is found, compares very well with neutron scattering experiments [9] and allowed us to study structural as well as dynamic properties of BPA-PC melts for systems up to 200 chains up to 20 entanglement molecular weights ($N_e \approx 5$–6, $N = 120$), corresponding to system sizes of $(100\ \text{nm})^3$ [20,21].

2.1. Inverse mapping

In the previous section we gave a very short account on the structure based coarse graining procedure for amorphous polymers. Since the cg models are still fairly close to the original chemical structure we can also make the step back and reintroduce the chemical details of the chains. That then allows for a detailed comparison to microscopic experiments. It also opens the way to the anticipated scale hopping or adaptive resolution simulation. There are several options to reintroduce chemical details [6,7,13,17,21,22]. If the polymers consists of reasonably rigid (all-atom) fragments it is sufficient to fit these rigid all-atom units onto the corresponding cg chain segment coordinates. The atomistic fragments are taken from a pool of structures, that correctly reflect the statistical weight of those degrees of freedom (DOFs), i.e., ring flips, that are not resolved in the cg description. Then a very short equilibration run of a few ps is performed, where the individual atoms typically move a distance less than 1.5 Å. This is to be compared to the typical strand–strand distance of about 5 Å in a polymer melt or to the size of a monomer, which in the case of BPA-PC is about 11 Å. Thus this is just a very local rattling. The so derived structures compare very well to scattering experiments [21]. Together with the characteristic ratio this indicates that the obtained all-atom melts truly represent the experimental system, supporting the overall consistency of the approach. Note that this procedure does not require any fitting to experiment for the bonded part and, for the present case, not even for the nonbonded part! In a first application to phenol diffusion in BPA-PC [23] the polymer matrix was generated by the above procedure to host the added small molecules.

2.2. Dynamics

The structure-based mapping scheme fixes the length scaling by its very construction. Though one would expect the same the appropriate timescale is not obvious at all. cg simulations are usually analyzed in Lennard–Jones units ϵ, σ and τ. Using realistic values for these units (mass of a cg unit in the model, etc.) one can determine the time scale of the cg simulation. Giving the same mass to all cg beads results in $1\tau = 1.7$ ps for BPA-PC at the process temperature of 570 K and $1\tau = 1.0$ ps for PS at 463 K, respectively. While these are the intrinsic time scales of the cg models, it is not the correct time scale for the underlying chemical system [20,21]. Although on the cg level scaling properties of the dynamics, such as Rouse behavior for short chain melts and reptation behavior long chain melts is well reproduced and the entanglement length accurately predicted, the time scale has yet to be determined. The reason for that originates from the fact, that the polymer melt dynamics is dominated by the chain friction, which results from local interactions as well as packing and topological constraints. Because of that it is not possible to calculate the time scaling from the potential functions of the simulations. A pragmatic direct way is to match mean square displacements of short all or united atom chain melts to the cg simulations. Doing this not only gives the time scaling but also shows, down to what scale the cg description follows the appropriate molecular motion. In the case of BPA-PC at 570 K we find $1\tau \approx 30$ ps and that the cg displacements properly represent atomistic trajectories down to distances of about 10 Å, roughly the size of a monomer. Combining all this means that in our case we now have systems with about 800000 atoms for times of up to $5 \cdot 10^{-4}$ s at hand. Along these lines recently we also investigated a variety of problems related to polystyrene [16,24] and find $1\tau \approx 7.7$ ps. Taking this together gives us confidence that the structure based coarse graining approach yields solid information on the statics and dynamics of complicated polymeric melts. Estimates of the speedup for the current simulations are around 10^4 compared to brute force all atom simulations.

2.3. Extension to surfaces

This ansatz has been used to study a number of different physical problems, which otherwise would have been too time demanding [20,23]. In the case of a metal surface, such as Ni, however, specific interactions of fragments of the chains might lead to rather different morphologies, as shown for the example of BPA-PC [25] (see Fig. 2). There the above cg scheme was combined with an ab initio density functional MD study of specific surface interactions. For this the monomer had to be cut into pieces and the interaction of the submolecules benzene and phenol, carbonic acid and propane with a Ni(1, 1, 1) surface was studied [15]. Because both carbonic acid and propane are strongly repelled by the Ni surface the strong attraction experienced by benzene is screened within the chain. This leads to the situation where only the terminal benzenes can adsorb. To show that this adsorption is very strong and compatible with the chemical structure of the chain, the full angular resolution at the carbonate unit next to the terminating benzene had to be considered. The comparison of different chain ends shows that the melt morphology close to the surface for phenolic chain ends is significantly different from the generic dispersion force dominated structure [15]. This has also been extended to study the sliding of BPA-PC melts under shear with and without additives [26–28] and at a surface defect [29].

3. Adaptive resolution simulation

3.1. Motivations

In the previous section a systematic coarse graining procedure was introduced, which allowed to efficiently simulate a system on a lower level of resolution while keeping the option to reintroduce the chemical details whenever needed. This methodology, however, applies to the whole system. What instead would be highly desirable is an approach, where (two) levels of resolution can be applied at the same time within one simulation in different areas and where both regimes are in true equilibrium with each other, allowing for a free exchange of molecules. Then one could run a simulation on a lower level of detail and zoom in on-the-fly, whenever "something interesting" happens. Theoretical methods employed to study such systems span from quantum-mechanical to macroscopic statistical approaches [15,25,30–33]. However, the common feature and limitation of all these methods is the fact that the regions or parts of the system treated at different level of resolution are fixed and do *not* allow for exchange of particles. Recently, we proposed the particle-based Adaptive Resolution Scheme (AdResS) [34] for hybrid all-atom/coarse-grained molecular dynamics (MD) simulations that fulfills the above requirement. The basic idea of this approach leads to the generalization of the equipartition theorem to non-integer dimensions of the phase space [35].

3.2. Adaptive resolution scheme (AdResS)

To concurrently couple the atomic and mesoscopic regimes within one single simulation, we developed the AdResS scheme [34], which is a two-stage procedure. Firstly, one has to define the cg sites/model and derive the effective pair potential U^{cg} between coarse-grained molecules such that the statistical properties, i.e., the density, pressure, and temperature, of the corresponding all-atom system are accurately reproduced. This can be done, e.g., along the lines described in the previous chapters. For practical reasons, as we will see later it is also advisable to match the radial distribution functions as closely as possible.[2] To determine the interactions, one can follow the schemes discussed in the previous section. Secondly, we introduce an interface layer (the transition regime) between the atomistic and coarse-grained regions, which contains hybrid molecules as illustrated in Fig. 3(a) for the simple example of tetrahedral liquid molecules (consider the middle "molecule") [34]. There each hybrid molecule corresponds to all-atom molecule with an additional massless center-of-mass particle serving as an interaction site. The transition is then governed by a weighting function $w(x) \in [0, 1]$ that interpolates the molecular interaction forces between the two regimes, and assigns the identity of the molecule [34]. $w(x)$ is defined in such a way that $w = 1$ corresponds to high resolution, $w = 0$ to low resolution, and

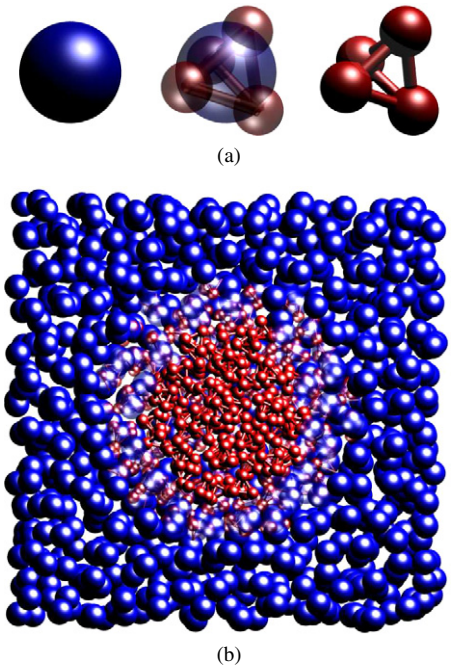

Fig. 3. (a) The on-the-fly interchange between the atomistic and coarse-grained levels of description. The middle hybrid molecule is a linear combination of fully atomistic molecule with an additional center of mass particle representing the coarse-grained molecule. (b) Snapshot of the hybrid atomistic/mesoscopic model liquid with $\rho = 0.175$ and $T = 1.0$. The red molecules are the explicit atomistically resolved tetrahedral molecules, the blue molecules are the corresponding one particle coarse-grained molecules. (For interpretation of the references to color in this figure legend, the reader is referred to the web version of this article.)

values $0 < w < 1$ to the transition regime, respectively. Interpolating forces and *not* potentials acting between centers of mass of molecules α and β [34] leads to:

$$\mathbf{F}_{\alpha\beta} = w(x_\alpha)w(x_\beta)\mathbf{F}^{\mathrm{ex}}_{\alpha\beta} + \big[1 - w(x_\alpha)w(x_\beta)\big]\mathbf{F}^{\mathrm{cg}}_{\alpha\beta}. \tag{2}$$

$\mathbf{F}_{\alpha\beta}$ is the total intermolecular force acting between centers of mass of the molecules α and β. $\mathbf{F}^{\mathrm{ex}}_{\alpha\beta}$ is the sum of all pair atom interactions between explicit atoms of the molecule α and explicit atoms of the molecule β, $\mathbf{F}^{\mathrm{cg}}_{\alpha\beta} = -\nabla U^{\mathrm{cg}}_{\alpha\beta}$ is the effective pair force between the two molecules, and x_α and x_β are the x center of mass coordinates of the molecules α and β. As given by Eq. (2), AdResS by construction satisfies Newton's Third Law, among others crucial for the proper diffusion of molecules across the resolution boundaries [36]. Since the total forces between the molecules, as defined by Eq. (2), depend on the absolute positions of the molecules and not only on their relative distances it is not conservative and the corresponding potential does not exist [37]. The work done by this force depends on the physical path taken by the respective hybrid molecule in the transition regime, i.e. on the number of particle collisions encountered on the way. However, despite the fact that within the AdResS scheme one cannot define the free energy in the transition region, the grand-canonical potential $\Omega = -pV$ is nevertheless a well defined and conserved quantity in our approach. In this way the all-atom part of the liquid is maintained at thermodynamical equilibrium with a far simpler coarse-grained fluid, i.e., spurious fluxes are avoided at the

[2] This actually allows to easily zoom in on a cg simulation on-the-fly, wherever this is of interest.

boundary between the atomistic and coarse-grained regimes. Each time a molecule crosses a boundary between the different regimes it gains or loses on-the-fly (depending on whether it leaves or enters the coarse-grained region) its equilibrated rotational and vibrational DOFs (present example) while retaining its linear momentum [35,38]. This change in resolution requires to supply or remove "latent heat" and thus must be accompanied with a thermostat that couples *locally* to the particle motion, e.g., Langevin or Dissipative Particle Dynamics (DPD) thermostats [39]. Furthermore, to properly define thermodynamics quantities, e.g., temperature, in the transition regime, where the number of DOFs varies, one has to resort to fractional calculus [35,36]. This leads then, for example, to a generalization of the equipartition theorem to the non-integer DOFs.

One could also attempt to introduce a mixing scheme along Eq. (2) directly on the interaction potentials rather than the forces [40]. It can be shown [35,36,41], however, that this leads to a violation of Newton's Third Law and consequently to non-conservation of the linear momentum.

3.3. Applications

Thus far, we have applied the AdResS scheme to a liquid of non-polar tetrahedral molecules, a generic model of a solvated macromolecule, and liquid water [34,42–44]. We carried out all of our hybrid multiscale simulations using a special modification of the ESPResSo package [45].

3.3.1. Liquid of tetrahedral molecules

The first test and proof of principle dealt with a liquid of simple model tetrahedral molecules [34] mentioned before. This model liquid mimics a typical liquid like methane [40,46], etc. Each molecule in this system is composed of four equal atoms with mass m_0. Their size σ is fixed via a repulsive Weeks–Chandler–Andersen (WCA) potential

$$U^{\mathrm{ex}}_{\mathrm{rep}}(r_{i_\alpha j_\beta}) = \begin{cases} 4\varepsilon\left[\left(\dfrac{\sigma}{r_{i_\alpha j_\beta}}\right)^{12} - \left(\dfrac{\sigma}{r_{i_\alpha j_\beta}}\right)^{6} + \dfrac{1}{4}\right]; & r_{i_\alpha j_\beta} \leqslant 2^{1/6}\sigma, \\ 0; & r_{i_\alpha j_\beta} > 2^{1/6}\sigma \end{cases} \tag{3}$$

with the cutoff at $2^{1/6}\sigma$, σ and ε being the standard Lennard–Jones parameters of length and energy. $r_{i\alpha j\beta}$ is the distance between the atom i of the molecule α and the atom j of the molecule β. All atoms of a molecule are connected by FENE bonds

$$U^{\mathrm{ex}}_{\mathrm{bond}}(r_{i_\alpha j_\alpha}) = \begin{cases} -\dfrac{1}{2}kR_0^2 \ln\left[1 - \left(\dfrac{r_{i_\alpha j_\alpha}}{R_0}\right)^2\right]; & r_{i_\alpha j_\alpha} \leqslant R_0, \\ \infty; & r_{i_\alpha j_\alpha} > R_0 \end{cases} \tag{4}$$

with $R_0 = 1.5\sigma$ and $k = 30\varepsilon/\sigma^2$. For technical details see Refs. [34,42].

In these tests a medium density liquid with an atom density of $\rho = 0.1/\sigma_{\mathrm{cg}}^3$ (corresponding to $\rho_{\mathrm{cg}} \approx 0.57/\sigma^3$) [34], and a high density liquid with $\rho = 0.175/\sigma^3 \approx 1.0/\sigma_{\mathrm{cg}}^3$ (σ_{cg} is the excluded volume diameter of the coarse-grained molecule) was treated in a slab like and in a cavity like geometry [42], see Fig. 3. In the remainder of the paper we use, if not specified differently, the dimensionless Lennard–Jones units [47].

The first step is to map the explicit atomistic (ex) model to a coarse-grained (cg) mesoscopic model. The latter is composed of N one-particle molecules schematically depicted in Fig. 3(a) (consider only the left blue molecule). The given coarse-grained molecules α have the same mass $M_\alpha = 4m_0$ as the explicit tetrahedral molecule. All rotational and vibrational DOFs of atomistically resolved tetrahedral molecules are thus removed, and the number of nonbonded interactions is strongly decreased as well. We derive the effective density and temperature dependent cg potential $U^{\mathrm{cg}}(r)$ in such a way that the center-of-mass radial distribution function ($\mathrm{RDF}_{\mathrm{cm}}$) (and thus the density) and pressure of the cg system match to the corresponding $\mathrm{RDF}_{\mathrm{cm}}$ and pressure of the ex system at a given density and temperature [48]. For the effective pair potential derivation one can resort to various methods found in the literature, see, e.g., Refs. [18,19,49]. This means that at the chosen state point the equations of state for the ex and cg systems coincide. The effective pair potential acting between the coarse-grained molecules is significantly softer than the pair potential between atoms of the resolved molecules [34,42], since it mimics a collection of atoms [50,51].

The $\mathrm{RDF}_{\mathrm{cm}}$s and equations of state for ex and cg systems, which are run using the tabulated effective potential, parameterized for $\rho = 0.175$, are displayed in Figs. 4(a) and 4(b), respectively [42]. The two $\mathrm{RDF}_{\mathrm{cm}}$s match to the line thickness. We can also see that the equations of state now, as expected, coincide around the state points the effective potentials were parameterized for.

In the next step, the atomistic and mesoscopic system are coupled via Eq. (2). The weighting function $w(x)$ for the slab like geometry or $w(r)$ for the spherical cavity like geometry has the shape of a $\cos^2$ or $\sin^2$ function in order to smoothly interpolate between the regimes and to have zero slope at the boundaries $\pm d$ of the transition regime. In order to avoid any kinetic barrier for a free exchange of particles, the density profile should be totally flat, also throughout the transition regime. There is however no reason, why any linear combination of two completely different set of forces based on completely different interaction potentials should result in exactly the same pressure and density. Indeed the pressure in a system containing exclusively hybrid molecules with constant $w \neq 0, 1$ slightly depends on the w value [34]. The increase in pressure is most prominent for $w = 1/2$, indicating that the most artificial case for the hybrid molecule is the mixture of $1/4$ of all-atom and $3/4$ of coarse-grained molecule. This justifies the asymmetric choice of using the switching factors $w(x_\alpha)w(x_\beta)$ and $1 - w(x_\alpha)w(x_\beta)$ in Eq. (2); this worst case occurs precisely in the middle of the transition regime, least affecting the all-atom and coarse-grained regimes.

To reduce the density and pressure fluctuations one can introduce a pressure correction function $s(w(x_\alpha)w(x_\beta))$ for the interpolation of the effective pair forces, $\mathbf{F}^{\mathrm{cg}}_{\alpha\beta}$, between coarse-grained molecules [42]. Fig. 5 displays the results of the density

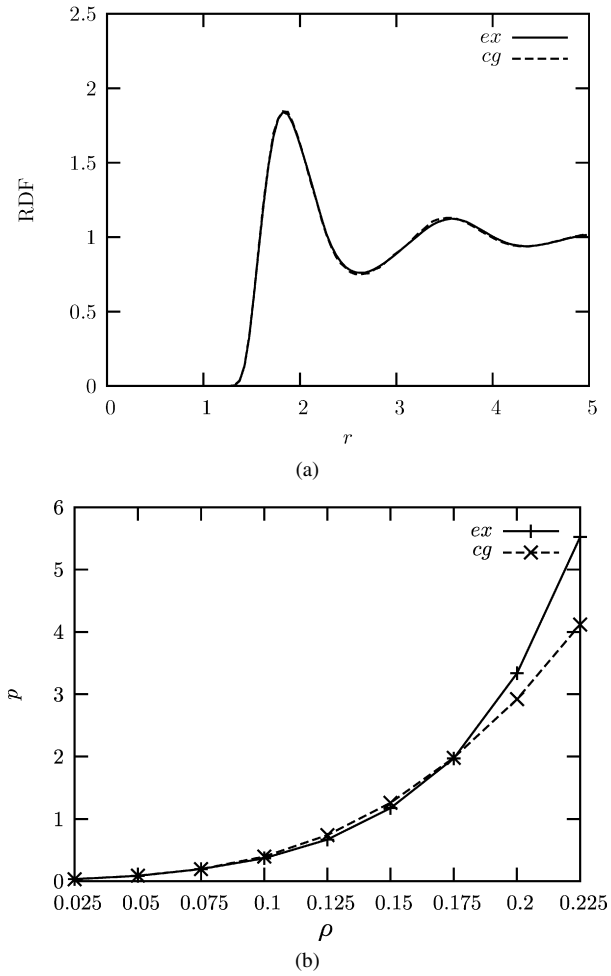

Fig. 4. (a) $\mathrm{RDF_{cm}}$ the ex and cg systems at $T = 1$ and $\rho = 0.175$. (b) Equation of state for the ex and cg systems at $T = 1$ and $\rho = 0.175$. Shown is the pressure p as a function of the number density ρ of the system, after Ref. [42].

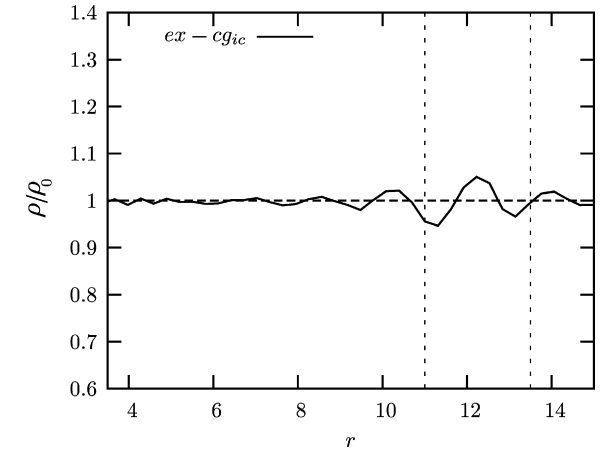

Fig. 5. The normalized radial number density profiles of the ex-$\mathrm{cg_{ic}}$ system at $\rho = 0.175$ and $T = 1$ for the radius of the explicit regime $r_0 = 11.0$. Vertical lines denote boundaries between atomistic, coarse-grained and interface regions of the system, after Ref. [42].

profile for the hybrid system with a simple single point version $s[y] = 4(\sqrt{y} - \frac{1}{2})^2$ of "the interface pressure correction" employed (ex-$\mathrm{cg_{ic}}$). Doing that involves a reparametrization of the

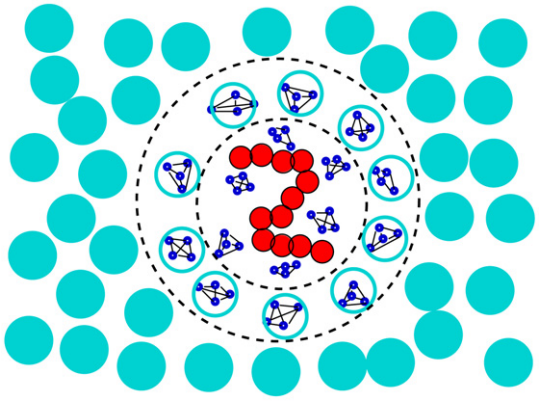

Fig. 6. A schematic plot of a solvated generic bead-spring polymer. The polymer beads are represented smaller than the solvent molecules for presentation convenience, for details see Ref. [43].

effective pair interaction in the system composed of exclusively hybrid molecules with the constant $w = 1/2$ over the whole system. In principle one can arrive at a completely flat density profile by applying multiple point versions of s.

3.3.2. Solvated macromolecule in a moving cell

The next example a polymer chain is surrounded by solvent with "atomistic" resolution, while further away the solvent is coarse grained as illustrated in Fig. 6 [43]. When the chain moves around, the sphere of atomistic resolution moves together with the center of mass of the chain. By this the chain is free to move around, although the explicit resolution sphere is much smaller than the overall simulation volume. Thus only the solvent in the vicinity of the macromolecule is always represented with a sufficiently high level of detail so that the specific interactions between a solvent and a solute are correctly taken into account. Solvent further away from the polymer, where the high resolution is no longer required, is represented on a more coarse-grained level. Here the macromolecule is represented by a generic flexible polymer chain [52] embedded in a solvent of the tetrahedral molecules introduced the previous section. In order to also make some first steps to the study of dynamics and to conserve momentum the particle motion was coupled to the DPD thermostat [39]. With $\mathbf{R}_\alpha$, $\mathbf{R}_\beta$, and $\mathbf{R}$ being the centers of mass of the molecules α, β and the whole polymer, respectively the AdResS scheme of Eq. (2) is generalized to:

$$\mathbf{F}_{\alpha\beta} = w\big(|\mathbf{R}_\alpha - \mathbf{R}|\big)w\big(|\mathbf{R}_\beta - \mathbf{R}|\big)\mathbf{F}^{\mathrm{ex}}_{\alpha\beta} + \big[1 - w\big(|\mathbf{R}_\alpha - \mathbf{R}|\big)w\big(|\mathbf{R}_\beta - \mathbf{R}|\big)\big]\mathbf{F}^{\mathrm{cg}}_{\alpha\beta}, \tag{5}$$

to take into account the moving of the high resolution scheme with the polymer. The size of the sphere is set such that the fluctuating polymer is always surrounded by the explicit solvent molecules. Thus, Eq. (5) for the forces in the transition regime only applies to the solvent.

In Fig. 7 polymer structure function $S(q)$ of the all explicit simulation is compared to the hybrid simulation scheme with (ex-$\mathrm{cg_{ic}}$) and without (ex-cg) the interface pressure correction applied in the transition regime for $N = 30$ beads and a cavity radius of $r_0 = 12.0\sigma$. As shown the chain conformations

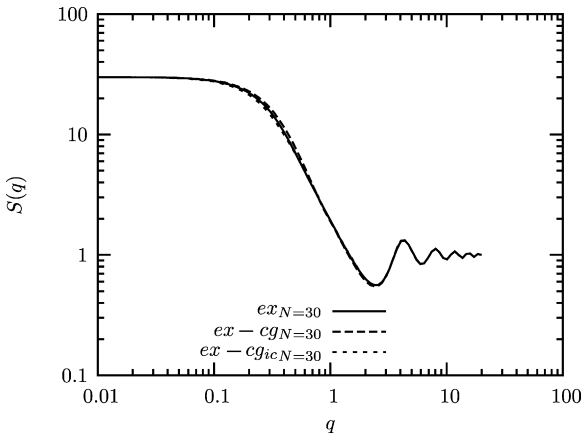

Fig. 7. The static structure factor of the polymer with $N = 30$ for the ex, ex-cg, and ex-cg_{ic} solvents, after Ref. [43].

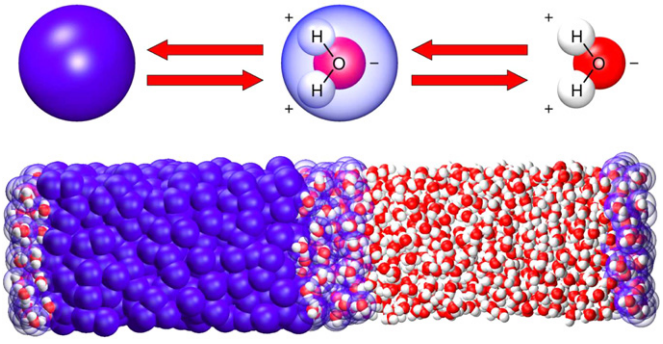

Fig. 8. (a) On-the-fly interchange between the all-atom and coarse-grained water models. (b) A schematic representation of the hybrid liquid water system, after Ref. [44].

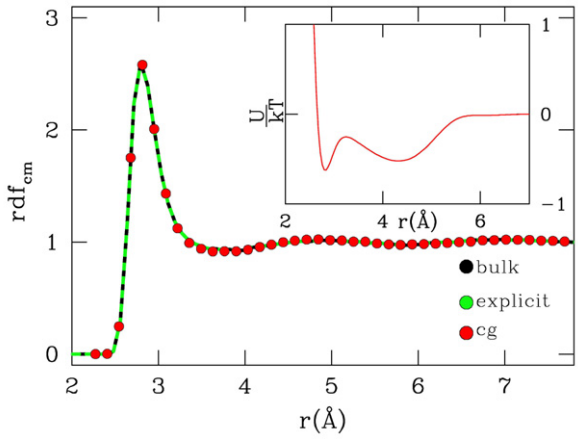

Fig. 9. The center-of-mass RDFs for explicit (ex) [green line] and coarse-grained (cg) [red line] regions of the hybrid system, are shown together with the RDFs corresponding to a bulk all-atom simulation (black line). The local O–H and H–H RDFs for the explicit molecules in the hybrid system compare equally well to the standard bulk simulations (not shown). The optimized effective potential for the coarse-grained model is shown in the inset as a function of inter-particle separation, r, after Ref. [44]. (For interpretation of the references to color in this figure legend, the reader is referred to the web version of this article.)

are not affected at all. The resulting diffusion constants of the chains increase due to the reduced viscosity of the cg liquid as we find, e.g., $D(\text{ex}) = 0.0030$ compared to $D(\text{ex-cg}) = 0.0035$. To improve this we are currently testing new local thermostats for molecular dynamics simulations [53], which will be shortly discussed below.

3.3.3. Liquid water

In this section the approach is extended to a model of liquid water [44] as depicted in Fig. 8.

The long-range electrostatic interactions are taken into account using the reaction field (RF) method, in which all molecules with the charge center outside a spherical cavity of a molecular based cutoff radius $R_c = 9$ Å are treated as a dielectric continuum with a dielectric constant ϵ_{RF} [54–56]. The Coulomb force acting on a charge e_{i_α}, at the center of the cutoff sphere, due to a charge e_{j_β} within the cavity is:

$$\mathbf{F}^{\text{ex}}_{C_{i_\alpha j_\beta}}(\mathbf{r}_{i_\alpha j_\beta}) = \frac{e_{i_\alpha} e_{j_\beta}}{4\pi\epsilon_0}\left[\frac{1}{r^3_{i_\alpha j_\beta}} - \frac{1}{R_c^3}\frac{2(\epsilon_{\text{RF}}-1)}{1+2\epsilon_{\text{RF}}}\right]\mathbf{r}_{i_\alpha j_\beta}. \quad (6)$$

This allows us to introduce a new simple single site water model in the cg regime, which contains no dipole moment. The single-site water model reproduces remarkably well the essential thermodynamic and structural features of water, as obtained by detailed all-atom simulations using the rigid TIP3P [57] water model. To derive the effective potential between cg molecules we follow an iterative inverse statistical mechanics approach proposed by Lyubartsev et al. [18], see Fig. 9. A perfect agreement between the all-atom and coarse-grained RDF_{cm}s is reached using the optimized effective potential (shown in the inset of Fig. 9). The effective potential has a first primary minimum at about 2.8 Å; corresponding to the first peak in the center-of-mass RDF. The slightly weaker and significantly broader minimum at 4.5 Å corresponds to the second hydration shell. The combined effect of the two minima leads to a local packing close to that of the all-atom TIP3P water. The normalized density for the hybrid system is homogeneous in the coarse-grained and explicit regions with (very) small oscillations in the transition regime, cf. Fig. 10. Along these lines AdResS can be applied to any other flexible or rigid nonpolarizable classical water model, e.g., SPC, SPC/E or TIP4P [56, 58–61].

The free exchange of molecules between the different regimes is illustrated by we the time evolution of a diffusion profile for molecules that were initially localized at the interface layer. Fig. 10 shows that these molecules spread out asymmetrically with time. This asymmetry arises from the aforementioned difference in diffusion coefficient between the all-atom and coarse-grained regions. However, one can adjust the diffusion coefficient of the coarse-grained molecules by using either the position dependent friction coefficient of the Langevin thermostat [62] or a new recently proposed Transverse DPD thermostat [53]. Whereas the Langevin thermostat screens off all hydrodynamic interactions, the Transverse DPD thermostat allows for tuning transport properties of fluids while preserving the hydrodynamics. This is achieved by coupling the DPD thermostat to the perpendicular components of relative velocities (see Fig. 11), while conventional DPD couples

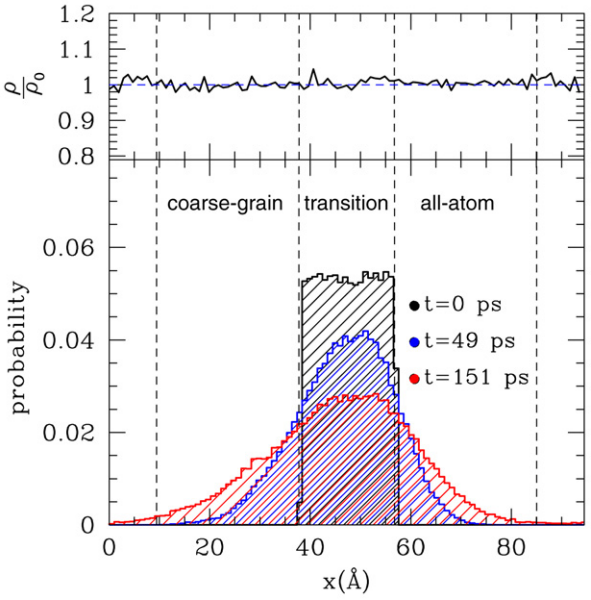

Fig. 10. Top: normalized density profile in the x-direction of the hybrid system. Bottom: Time evolution of a diffusion profile for the molecules that are initially (at time $t = 0$ ps) located in the interface region. The diffusion profile is averaged over ≈ 400 different time origins. Vertical lines denote the boundaries of the interface layer, from Ref. [44].

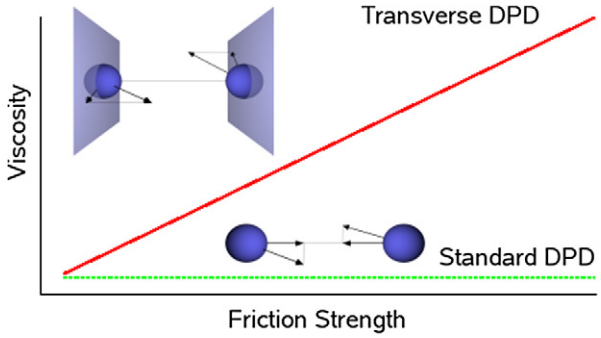

Fig. 11. The Transverse DPD thermostat allows for controlling the transport properties of liquids while preserving the stabilizing and hydrodynamics properties of the system, after Ref. [53].

to the relative velocities parallel to their distance vector. Of course this idea can readily be applied to regular DPD simulations as well, which treat large soft particles by Brownian dynamics [63–66].

4. Conclusions

Many interesting problems in (soft) condensed matter are inherently multiscale and it is exactly this scale interplay that drives the relevant properties of the system. While analytic theory here can only be very approximative, computer simulations can address this issue via time and length scale bridging techniques [14]. Quantum, classical atomistic and coarse grained scales can be linked in a consistent sequential way to account for the different level of detail and to reduce the computational effort massively. The example of polycarbonate in bulk and at a metal surface illustrates this situation. It represents a typical case of coupling specific interactions at the surface (quantum scale) and global conformations (classical atomistic coarse grained level). In the case of polycarbonate it was sufficient to only keep the full atomistic angular resolution of the chemical bonds for the phenol at the chain end. This did not affect the efficiency of the simulation significantly. However usually the requirement of more detail applies to all parts of a macromolecule close to a surface with specific interactions. That are exactly those problems that ask for new computational schemes which can take into account simultaneously all relevant scales involved only in a region of space, where they are needed. Specifically, the question arises, whether one can devise an adaptive resolution method, which allows to treat different regions with different resolutions, yet allowing the free exchange of particles among such regions? For a macromolecule–surface system, as a bead approaches the surface it slowly acquires the atomistic structure (and loses the coarse-grained one), while doing the opposite when moving away form the surface. One possible solution to that problem is represented by the AdResS method. The method allows to change degrees of freedom on the fly during a simulation run and thus allows us to adaptively change the resolution of the molecule in given region of space but keeping the free exchange of molecules among the regions of different resolution. So far this approach technical prototypes, which serve as tests for applications such as solvation of large molecules and surface–polymer systems.

Acknowledgements

Over the years we have enjoyed the collaboration with many colleagues and students on the topics described in this short overview. Out of them we would like to especially thank C.F. Abrams, S. Leon, F. Müller-Plathe, N. van der Vegt, C. Peter, B. Hess, V. Harmandaris, C. Clementi, S. Matysiak and the ESPResSo team for fruitful collaboration and many discussions. This research in part was supported within the BMBF Center on Multiscale Materials Simulations, the Volkswagen Foundation and the Bayer AG and BASF AG.

References

[1] P.J. Flory, Principles of Polymer Chemistry, Cornell University Press, Ithaca, 1953.
[2] P.J. Flory, Statistical Mechanics of Chain Molecules, Interscience Publishers, New York, 1969.
[3] P.-G. de Gennes, Scaling Concept in Polymer Physics, Cornell University, Ithaca, 1979.
[4] M. Doi, S.F. Edwards, The Theory of Polymer Dynamics, Clarendon, Oxford, 1986.
[5] K. Binder (Ed.), Monte Carlo and Molecular Dynamics Simulation in Polymer Science, Clarendon, Oxford, 1995.
[6] W. Tschöp, K. Kremer, J. Batoulis, T. Bürger, O. Hahn, Simulation of polymer melts. I. Coarse-graining procedure for polycarbonates, Acta Polym. 49 (1998) 61–74.
[7] W. Tschöp, K. Kremer, O. Hahn, J. Batoulis, T. Bürger, Simulation of polymer melts. II. From coarse-grained models back to atomistic description, Acta Polym. 49 (1998) 75–79.
[8] K. Kremer, Computer simulations in soft matter science, in: M.E. Cates, M.R. Evans (Eds.), Soft and Fragile Matter, Nonequilibrium Dynamics,

Metastability and Flow, Proceedings of NATO ASI Workshop, St. Andrews, Summer 1999, Inst. of Physics, Bristol, 2000.
[9] J. Eilhard, A. Zirkel, W. Tschöp, O. Hahn, K. Kremer, O. Scharpf, D. Richter, U. Buchenau, Spatial correlations in polycarbonates: Neutron scattering and simulation, J. Chem. Phys. 110 (1999) 1819–1830.
[10] C.F. Abrams, K. Kremer, Combined coarse-grained and atomistic simulation of liquid bisphenol-a-polycarbonate: Liquid packing and intramolecular structure, Macromolecules 36 (2003) 260–267.
[11] M. Ferraio, G. Ciccotti, K. Binder (Eds.), Computer Simulations in Condensed Matter Systems: From Materials to Chemical Biology, vol. 1, Lecture Notes Phys., vol. 703, Springer, Berlin/Heidelberg, 2006.
[12] M. Ferraio, G. Ciccotti, K. Binder (Eds.), Computer Simulations in Condensed Matter Systems: From Materials to Chemical Biology, vol. 2, Lecture Notes Phys., vol. 704, Springer, Berlin/Heidelberg, 2006.
[13] N.F.A. van der Vegt, C. Peter, K. Kremer, Structure-based coarse- and fine-graining in soft matter simulations, in: G. Voth (Ed.), Coarse-Graining of Condensed Phase and Biomolecular Systems, Chapman and Hall/CRC Press, Taylor and Francis Group, 2007.
[14] M. Praprotnik, L. Delle Site, K. Kremer, Multiscale simulation of soft matter: From scale bridging to adaptive resolution, Annu. Rev. Phys. Chem. 59 (2008) 545–571.
[15] L. Delle Site, S. Leon, K. Kremer, BPA-PC on a Ni(111) surface: The interplay between adsorption energy and conformational entropy for different chain-end modifications, J. Amer. Chem. Soc. 126 (2004) 2944–2955.
[16] V. Harmandaris, D. Reith, N.F. van der Vegt, K. Kremer, Comparison between coarse-graining models for polymers systems: Two mapping schemes for polystyrene, Macromol. Chem. Phys. 208 (2007) 2109–2120.
[17] C.F. Abrams, L. Delle Site, K. Kremer, Dual-resolution coarse-grained simulation of the bisphenol-a-polycarbonate/nickel interface, Phys. Rev. E 67 (2003) 021807.
[18] A.P. Lyubartsev, A. Laaksonen, Calculation of effective interaction potentials from radial distribution functions: A reverse Monte Carlo approach, Phys. Rev. E 52 (1995) 3730–3737.
[19] D. Reith, M. Pütz, F. Müller-Plathe, Deriving effective mesoscale potentials from atomistic simulations, J. Comput. Chem. 24 (2003) 1624–1636.
[20] S. Leon, L. Delle Site, N.F.A. van der Vegt, K. Kremer, Bisphenol-a-polycarbonate: Entanglement analysis from coarse-grained MD simulations, Macromolecules 38 (2005) 8078–8092.
[21] B. Hess, S. Leon, N. Van der Vegt, K. Kremer, Long time atomistic polymer trajectories from coarse grained simulations: bisphenol-a-polycarbonate, Soft Matter 2 (2006) 409–414.
[22] A.P. Heath, L.E. Kavraki, C. Clementi, From coarse-grain to all-atom: Toward multiscale analysis of protein landscapes, Proteins Struct. Funct. Bioinf. 68 (2007) 646–661.
[23] O. Hahn, D.A. Mooney, F. Müller-Plathe, K. Kremer, A new mechanism for penetrant diffusion in amorphous polymers: Molecular dynamics simulations of phenol diffusion in bisphenol-a-polycarbonate, J. Chem. Phys. 111 (1999) 6061–6068.
[24] V.A. Harmandaris, N.P. Adhikari, N.F.A. Van der Vegt, K. Kremer, Hierarchical modeling of polystyrene: From atomistic to coarse-grained simulations, Macromolecules 39 (2006) 6708–6719.
[25] L. Delle Site, C.F. Abrams, A. Alavi, K. Kremer, Polymers near metal surfaces: Selective adsorption and global conformations, Phys. Rev. Lett. 89 (2002) 156103.
[26] X. Zhou, D. Andrienko, L. Delle Site, K. Kremer, Dynamics surface decoupling in a sheared polymer melt, Europhys. Lett. 70 (2005) 264–270.
[27] X. Zhou, D. Andrienko, L. Delle Site, K. Kremer, Flow boundary conditions for chain-end adsorbing polymer melts, J. Chem. Phys. 123 (2005) 104904.
[28] D. Andrienko, S. Leon, L. Delle Site, K. Kremer, Adhesion of polycarbonate blends on a nickel surface, Macromolecules 38 (2005) 5810–5816.
[29] L. Delle Site, S. Leon, K. Kremer, Specific interaction of polymers with surface defects: Structure formation of polycarbonate on nickel, J. Phys.: Condens. Matter 17 (2005) L53–L60.
[30] A. Malevanets, R. Kapral, Solute molecular dynamics in a mesoscale solvent, J. Chem. Phys. 112 (2000) 7260–7269.
[31] E. Villa, A. Balaeff, L. Mahadevan, K. Schulten, Multiscale method for simulating protein-DNA complexes, Multiscale Model. Simul. 2 (2004) 527–553.
[32] M. Neri, C. Anselmi, M. Cascella, A. Maritan, P. Carloni, Coarse-grained model of proteins incorporating atomistic detail of the active site, Phys. Rev. Lett. 95 (2005) 218102.
[33] A. Laio, J. VandeVondele, U. Röthlisberger, A Hamiltonian electrostatic coupling scheme for hybrid Car–Parrinello molecular dynamics simulations, J. Chem. Phys. 116 (2002) 6941.
[34] M. Praprotnik, L. Delle Site, K. Kremer, Adaptive resolution molecular dynamics simulation: Changing the degrees of freedom on the fly, J. Chem. Phys. 123 (2005) 224106.
[35] M. Praprotnik, K. Kremer, L. Delle Site, Adaptive molecular resolution via a continuous change of the phase space dimensionality, Phys. Rev. E 75 (2007) 017701.
[36] M. Praprotnik, K. Kremer, L. Delle Site, Fractional dimensions of phase space variables: A tool for varying the degrees of freedom of a system in a multiscale treatment, J. Phys. A: Math. Theor. 40 (2007) F281–F288.
[37] H. Goldstein, Classical Mechanics, second ed., Addison-Wesley Publishing Company, 1980.
[38] M. Praprotnik, D. Janežič, Molecular dynamics integration meets standard theory of molecular vibrations, J. Chem. Inf. Model 45 (2005) 1571–1579.
[39] T. Soddemann, B. Dünweg, K. Kremer, Dissipative particle dynamics: A useful thermostat for equilibrium and nonequilibrium molecular dynamics simulations, Phys. Rev. E 68 (2003) 046702.
[40] B. Ensing, S.O. Nielsen, P.B. Moore, M.L. Klein, M. Parrinello, Energy conservation in adaptive hybrid atomistic/coarse-grain molecular dynamics, J. Chem. Theory Comput. 3 (2007) 1100–1105.
[41] L. Delle Site, Some fundamental problems for an energy-conserving adaptive-resolution molecular dynamics scheme, Phys. Rev. E 76 (2007) 047701.
[42] M. Praprotnik, L. Delle Site, K. Kremer, Adaptive resolution scheme (address) for efficient hybrid atomistic/mesoscale molecular dynamics simulations of dense liquids, Phys. Rev. E 73 (2006) 066701.
[43] M. Praprotnik, L. Delle Site, K. Kremer, A macromolecule in a solvent: Adaptive resolution molecular dynamics simulation, J. Chem. Phys. 126 (2007) 134902.
[44] M. Praprotnik, S. Matysiak, L. Delle Site, K. Kremer, C. Clementi, Adaptive resolution simulation of liquid water, J. Phys.: Condens. Matter 19 (2007) 292201.
[45] H.J. Limbach, A. Arnold, B.A. Mann, C. Holm, Espresso—an extensible simulation package for research on soft matter systems, Comput. Phys. Comm. 174 (2006) 704–727, http://www.espresso.mpg.de.
[46] C.F. Abrams, Concurrent dual-resolution Monte Carlo simulation of liquid methane, J. Chem. Phys. 123 (2005) 234101.
[47] M.P. Allen, D.J. Tildesley, Computer Simulation of Liquids, Clarendon Press, Oxford, 1987.
[48] R.L. Henderson, A uniqueness theorem for fluid pair correlation functions, Phys. Lett. A 49 (1974) 197–198.
[49] S. Izvekov, G.A. Voth, Multiscale coarse graining of liquid-state systems, J. Chem. Phys. 123 (2005) 134105.
[50] S.H.L. Klapp, D.J. Diestler, M. Schoen, Why are effective potentials 'soft'? J. Phys.: Condens. Matter 16 (2004) 7331–7352.
[51] H. Bock, K.E. Gubbins, S.H.L. Klapp, Coarse graining of nonbonded degrees of freedom, Phys. Rev. Lett. 98 (2007) 267801.
[52] K. Kremer, G.S. Grest, Dynamics of entangled linear polymer melts: A molecular-dynamics simulation, J. Chem. Phys. 92 (1990) 5057–5086.
[53] C. Junghans, M. Praprotnik, K. Kremer, Transport properties controlled by a thermostat: An extended dissipative particle dynamics thermostat, Soft Matter 4 (2008) 156–161.
[54] M. Neumann, The dielectric constant of water. computer simulations with the MCY potential, Mol. Phys. 50 (1983) 841.
[55] M. Neumann, The dielectric constant of water. Computer simulations with the MCY potential, J. Chem. Phys. 82 (1985) 5663–5672.
[56] M. Praprotnik, D. Janežič, J. Mavri, Temperature dependence of water vibrational spectrum: A molecular dynamics simulation study, J. Phys. Chem. A 108 (2004) 11056–11062.

[57] W.L. Jorgensen, J. Chandrasekhar, J.D. Madura, R.W. Impey, M.L. Klein, Comparison of simple potential functions for simulating liquid water, J. Chem. Phys 79 (1983) 926–936.
[58] H.J.C. Berendsen, J.P.M. Postma, W.F. van Gunsteren, J. Hermans, Molecular dynamics simulations: The limits and beyond, in: B. Pullman (Ed.), Intermolecular Forces, Reidel, Dordrecht, 1981, p. 331.
[59] H.J.C. Berendsen, J.R. Grigera, T.P. Straatsma, The missing term in effective pair potentials, J. Phys. Chem. 91 (1987) 6269–6271.
[60] C.P. Lawrence, J.L. Skinner, Flexible TIP4P model for molecular dynamics simulation of liquid water, Chem. Phys. Lett. 372 (2003) 842–847.
[61] M.E. Johnson, T. Head-Gordon, A.A. Louis, Representability problems for coarse-grained water potentials, J. Chem. Phys. 126 (2007) 144509.
[62] S. Matysiak, C. Clementi, M. Praprotnik, K. Kremer, L. Delle Site, Modeling diffusive dynamics in adaptive resolution simulation of liquid water, J. Chem. Phys. 128 (2008) 024503.
[63] P.J. Hoogerbrugge, J.M.V.A. Koelman, Simulating microscopic hydrodynamic phenomena with Dissipative particle dynamics, Europhys. Lett. 19 (1992) 155–160.
[64] P. Español, P. Warren, Statistical mechanics of dissipative particle dynamics, Europhys. Lett. 30 (1995) 191–196.
[65] R.D. Groot, P.B. Warren, Dissipative particle dynamics: Bridging the gap between atomistic and mesoscopic simulation, J. Chem. Phys. 107 (1997) 4423–4435.
[66] P. Español, Fluid particle model, Phys. Rev. E 57 (1998) 2930–2948.